

# Quantum phase transition triggering magnetic BICs in graphene

L. H. Guessi<sup>1</sup>, Y. Marques<sup>2</sup>, R. S. Machado<sup>2</sup>, K. Kristinsson<sup>3</sup>,

L. S. Ricco<sup>2</sup>, I. A. Shelykh<sup>3,4,5</sup>, M. S. Figueira<sup>6</sup>, M. de Souza<sup>1,\*</sup> and A. C. Seridonio<sup>1,2</sup>

<sup>1</sup>IGCE, Unesp - Univ Estadual Paulista, Departamento de Física, 13506-900, Rio Claro, SP, Brazil

<sup>2</sup>Departamento de Física e Química, Unesp - Univ Estadual Paulista, 15385-000, Ilha Solteira, SP, Brazil

<sup>3</sup>Division of Physics and Applied Physics, Nanyang Technological University 637371, Singapore

<sup>4</sup>Science Institute, University of Iceland, Dunhagi-3, IS-107, Reykjavik, Iceland

<sup>5</sup>ITMO University, St. Petersburg 197101, Russia

<sup>6</sup>Instituto de Física, Universidade Federal Fluminense, 24210-340, Niterói, RJ, Brazil

Graphene hosting a pair of collinear adatoms in the phantom atom configuration has pseudogap with cubic scaling on energy,  $\Delta \propto |\varepsilon|^3$  which leads to the appearance of spin-degenerate bound states in the continuum (BICs) [Phys. Rev. B **92**, 045409 (2015)]. In the case when adatoms are locally coupled to a single carbon atom the pseudogap scales linearly with energy, which prevents the formation of BICs. In this Letter, we explore the effects of non-local coupling characterized by the Fano factor of interference  $q_0$ , tunable by changing the slope of the Dirac cones in the graphene band-structure. We demonstrate that three distinct regimes can be identified: i) for  $q_0 < q_{c1}$  (critical point) a mixed pseudogap  $\Delta \propto |\varepsilon|, |\varepsilon|^2$  appears yielding a phase with spin-degenerate BICs; ii) near  $q_0 = q_{c1}$  when  $\Delta \propto |\varepsilon|^2$  the system undergoes a quantum phase transition in which the new phase is characterized by magnetic BICs and iii) at a second critical value  $q_0 > q_{c2}$  the cubic scaling of the pseudogap with energy  $\Delta \propto |\varepsilon|^3$  characteristic to the phantom atom configuration is restored and the phase with non-magnetic BICs is recovered. The phase with magnetic BICs can be described in terms of an effective intrinsic exchange field of ferromagnetic nature between the adatoms mediated by graphene monolayer. We thus propose a new type of quantum phase transition resulting from the competition between the states characterized by spin-degenerate and magnetic BICs.

PACS numbers: 72.80.Vp, 07.79.Cz, 72.10.Fk

**Introduction.-** Graphene-based systems are promising candidates for the detection of the so-called bound states in the continuum (BICs) [1, 2]. BICs were first theoretically predicted by von Neumann and Wigner in 1929 [3] as quantum states with localized square-integrable wave functions, but having energies within the continuum of delocalized states. The electrons within BICs do not decay into the system continuum, thus these states should be invisible in transport experiments.

The subject experienced revival after the work of Stillinger and Herrick in 1975 [4]. Since then, BICs were predicted to appear in a variety of electronic, optical and photonic systems [1, 5, 6]. In these systems, effects of Fano interference [7] were proposed as the underlying mechanism for the emergence of BICs and their possible experimental observation. In particular, we recently proposed that BICs can be observed in the system of graphene with two collinear adatoms in the phantom atom configuration [1].

In this Letter, we show that similar system shown in Fig.1 can undergo a quantum phase transition into the state with magnetic BICs if non-local graphene-adatom couplings are taken into account. The phenomenon arises in the region with quadratic dependence of the pseudogap on energy  $\Delta \propto |\varepsilon|^2$  and is similar to the transition reported in Ref. [8] for a pair of quantum dots coupled to metallic leads.

The quantum phase transition reported here is driven by a Fano factor of interference  $q_0$  which can be thus con-

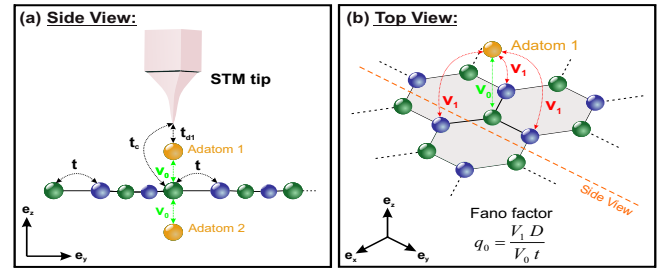


Figure 1: (Color online) Scheme of the setup proposed for the observation of a quantum phase transition in graphene. (a) Side view: two adatoms labeled by 1 (upper) and 2 (lower) placed collinear to a carbon atom beneath an STM tip. (b) Top view of the graphene-adatom subsystem. The adatoms are coupled to the carbon atom beneath them and its nearest neighbors. The relative strength of these couplings define the Fano factor of interference  $q_0$  playing the role of the natural order parameter of the system. See details in the main text.

sidered as the natural order parameter of the system. It can be tuned by changing the slope of the Dirac cones in the graphene band-structure. The magnetic BICs appear within the region inside the critical boundaries  $q_{c1} < q_0 < q_{c2}$ , where the dominant scaling law for the pseudogap is quadratic ( $\Delta \propto |\varepsilon|^2$ ). Outside this region, the mixed scaling  $\Delta \propto |\varepsilon|, |\varepsilon|^2$  for  $q_0 < q_{c1}$  or cubic scaling  $\Delta \propto |\varepsilon|^3$  for  $q_0 > q_{c2}$ , leads to the formation of spin-degenerate BICs. The transition towards the magnetic BIC state is triggered due to the onset of the effective

intrinsic ferromagnetic exchange field  $\mathcal{J}^{\text{exch}}$  between the adatoms mediated by the graphene monolayer.

*The model.*- To give a theoretical description of the setup plotted at Fig.1, we use the model based on the Anderson Hamiltonian [9, 10]:

$$\begin{aligned} \mathcal{H}_{2D} = & \sum_{s\sigma} \int dk (\hbar v_F k) c_{sk\sigma}^\dagger c_{sk\sigma} + \sum_{j\sigma} \varepsilon_{jd} d_{j\sigma}^\dagger d_{j\sigma} \\ & + \mathcal{U} \sum_j n_{d_j\uparrow} n_{d_j\downarrow} + \sum_{js\sigma} \int dk \mathcal{V}_k (c_{sk\sigma}^\dagger d_{j\sigma} + \text{H.c.}), \end{aligned} \quad (1)$$

with  $v_F$  being Fermi velocity. The graphene monolayer is described by operators  $c_{sk\sigma}^\dagger$  ( $c_{sk\sigma}$ ) for creation (annihilation) of electrons in quantum states labeled by the wave number  $k$ , spin  $\sigma$  and valley index  $s = 1, 2$ . For the adatoms,  $d_{j\sigma}^\dagger$  ( $d_{j\sigma}$ ) creates (annihilates) an electron with spin  $\sigma$  with energy  $\varepsilon_{jd}$ , where  $j = 1, 2$  correspond to the upper and lower adatoms, respectively. The third term in Eq.(1) accounts for the on-site Coulomb interaction  $\mathcal{U}$ , with  $n_{d_j\sigma} = d_{j\sigma}^\dagger d_{j\sigma}$ . Finally, the last term mixes the graphene and the levels  $\varepsilon_{jd}$ , wherein H.c. gives the Hermitian conjugate of the first part. This mixing is characterized by the coupling  $\mathcal{V}_k = \frac{1}{2\pi} \sqrt{\frac{\pi\Omega_0}{\mathcal{N}}} \sqrt{|k|} v_0 (1 - q_0 \frac{\hbar v_F k}{D})$ , where  $\mathcal{N}$  is the number of conduction states,  $\Omega_0$  denotes the unit cell area, and

$$q_0 = \frac{v_1 D}{v_0 t} \quad (2)$$

is the Fano factor of interference defined according to the results of Ref. [11]. The parameter  $t$  stands for the coupling strength between carbon atoms, while  $v_0$  and  $v_1$  represent the host-adatom hybridizations outlined in Fig.1 and  $D = 7\text{eV}$  denotes the band-edge. The Fano factor  $q_0$  changes as we vary  $v_F$  ( $t = \frac{2\hbar}{3a} v_F$  [12]) by keeping fixed the ratio  $\frac{v_1}{v_0}$  and the side length  $a$  of the hexagonal cells. The experimental tuning of  $v_F$  is achievable by changing the dielectric constant of the substrate where the graphene monolayer is deposited on [13]. The situation  $q_0 = 0$  corresponds to the scenario in which collinear adatoms are locally side-coupled to a single carbon atom (local coupling regime). Otherwise,  $q_0 \neq 0$  denotes the hybridization of the adatoms with the three second neighbors of carbons as depicted in Fig.1 (non-local coupling).

To determine the density of states  $\text{DOS}_{jj}^\sigma$  of the adatoms, we should calculate the Green's functions  $\tilde{\mathcal{G}}_{d_{j\sigma}d_{j\sigma}}$  ( $j = 1, 2$ ) and use the relation:

$$\text{DOS}_{jj}^\sigma = -\frac{1}{\pi} \text{Im}(\tilde{\mathcal{G}}_{d_{j\sigma}d_{j\sigma}}). \quad (3)$$

To this end, the Hubbard I approach is used [14]. We start employing the equation-of-motion method to a single particle retarded Green's function of an adatom in time domain  $\mathcal{G}_{d_{l\sigma}d_{j\sigma}} =$

$-\frac{i}{\hbar} \theta(\tau) \text{Tr}\{\varrho_{2D}[d_{l\sigma}(\tau), d_{j\sigma}^\dagger(0)]_+\}$ , where  $\theta(\tau)$  is the Heaviside function,  $\varrho_{2D}$  is the density matrix of the system described by the Hamiltonian of Eq.(1) and  $[\dots, \dots]_+$  is the anticommutator between operators taken in the Heisenberg picture. Performing elementary algebra one obtains in the energy domain:

$$\begin{aligned} (\varepsilon^+ - \varepsilon_{ld}) \tilde{\mathcal{G}}_{d_{l\sigma}d_{j\sigma}} &= \delta_{lj} + \Sigma \sum_{\bar{l}} \tilde{\mathcal{G}}_{d_{\bar{l}\sigma}d_{j\sigma}} \\ &+ \mathcal{U} \tilde{\mathcal{G}}_{d_{l\sigma}n_{d_{\bar{l}\sigma}}, d_{j\sigma}}, \end{aligned} \quad (4)$$

where  $\varepsilon^+ = \varepsilon + i0^+$  and

$$\begin{aligned} \Sigma &= \sum_s \int dk \frac{\mathcal{V}_k \mathcal{V}_k}{\varepsilon^+ - \hbar v_F k} = -\frac{v_0^2}{D^2} \varepsilon (1 - q_0 \frac{\varepsilon}{D})^2 \ln \left| \frac{D^2 - \varepsilon^2}{\varepsilon^2} \right| \\ &+ \frac{v_0^2}{D} q_0 (2 - q_0 \frac{\varepsilon}{D}) - i\Delta \end{aligned} \quad (5)$$

is the self-energy expressed in terms of the pseudogap [8]:

$$\Delta = \frac{\pi v_0^2}{D^2} |\varepsilon| (1 - q_0 \frac{\varepsilon}{D})^2, \quad (6)$$

which depending on the strength of  $q_0$  yields corresponding dominant scaling laws as we will see below. In Eq.(4)  $\tilde{\mathcal{G}}_{d_{l\sigma}n_{d_{\bar{l}\sigma}}, d_{j\sigma}}$  is a two particle Green's function composed by four fermionic operators, obtained from the time Fourier transform of  $\mathcal{G}_{d_{l\sigma}n_{d_{\bar{l}\sigma}}, d_{j\sigma}} = -\frac{i}{\hbar} \theta(\tau) \text{Tr}\{\varrho_{2D}[d_{l\sigma}(\tau) n_{d_{\bar{l}\sigma}}(\tau), d_{j\sigma}^\dagger(0)]_+\}$ , with  $n_{d_{\bar{l}\sigma}} = d_{l\bar{\sigma}}^\dagger d_{l\bar{\sigma}}$  and spin  $\bar{\sigma}$  (opposite to  $\sigma$ ). Thus we first calculate the time derivative of  $\mathcal{G}_{d_{l\sigma}n_{d_{\bar{l}\sigma}}, d_{j\sigma}}$  and then its time Fourier transform, which leads to

$$\begin{aligned} (\varepsilon^+ - \varepsilon_{ld} - \mathcal{U}) \tilde{\mathcal{G}}_{d_{l\sigma}n_{d_{\bar{l}\sigma}}, d_{j\sigma}} &= \delta_{lj} \langle n_{d_{\bar{l}\sigma}} \rangle \\ &+ \sum_s \int dk \mathcal{V}_k (\tilde{\mathcal{G}}_{c_{sk\sigma}d_{l\bar{\sigma}}^\dagger d_{l\bar{\sigma}}, d_{j\sigma}} \\ &- \tilde{\mathcal{G}}_{c_{sk\bar{\sigma}}^\dagger d_{l\bar{\sigma}} d_{l\sigma}, d_{j\sigma}} + \tilde{\mathcal{G}}_{d_{l\bar{\sigma}}^\dagger c_{sk\bar{\sigma}} d_{l\sigma}, d_{j\sigma}}), \end{aligned} \quad (7)$$

expressed in terms of new Green's functions of the same order of  $\tilde{\mathcal{G}}_{d_{l\sigma}n_{d_{\bar{l}\sigma}}, d_{j\sigma}}$  and the occupation number  $\langle n_{d_{\bar{l}\sigma}} \rangle$  determined by

$$\langle n_{d_{\bar{l}\sigma}} \rangle = -\frac{1}{\pi} \int_{-D}^{\varepsilon_F=0} \text{Im}(\tilde{\mathcal{G}}_{d_{l\bar{\sigma}}d_{l\bar{\sigma}}}) d\varepsilon. \quad (8)$$

Furthermore, by employing the Hubbard I approximation, we decouple the Green's functions in the right-hand side of Eq. (7) as performed in Ref. [1]. This procedure enables us to solve the system of Green's functions within Eq.(4), leading to  $\tilde{\mathcal{G}}_{d_{j\sigma}d_{j\sigma}} = \frac{\lambda_{jj}^\sigma}{\varepsilon - \varepsilon_{jd} - \Sigma_{jj}^\sigma}$ , where  $\lambda_{jj}^\sigma = (1 + \frac{\mathcal{U} \langle n_{d_{j\sigma}} \rangle}{\varepsilon - \varepsilon_{jd} - \mathcal{U} - \Sigma})$ , and:

$$\tilde{\Sigma}_{j\bar{j}}^{\bar{\sigma}} = \Sigma + \lambda_j^{\bar{\sigma}} \lambda_{\bar{j}}^{\bar{\sigma}} \frac{\Sigma^2}{\varepsilon - \varepsilon_{j\bar{d}} - \Sigma} \quad (9)$$

is the total self-energy, with  $\bar{j} = 2, 1$  respectively for  $j = 1, 2$  in order to identify distinct adatoms and  $\tilde{\mathcal{G}}_{d_j\sigma d_{\bar{j}}\sigma} = \frac{\lambda_j^{\bar{\sigma}} \Sigma \tilde{\mathcal{G}}_{d_{\bar{j}}\sigma d_{j\sigma}}}{\varepsilon - \varepsilon_{j\bar{d}} - \Sigma}$  are mixed Green's functions. To obtain the host local DOS (LDOS) probed by the STM tip of Fig. 1, we introduce the retarded Green's function in time coordinate  $\mathcal{G}_\sigma = -\frac{i}{\hbar} \theta(\tau) \text{Tr}\{\rho_{2D}[\Psi_\sigma(\tau), \Psi_\sigma^\dagger(0)]_+\}$ , with

$$\Psi_\sigma = \frac{1}{2\pi} \sqrt{\frac{\pi\Omega_0}{\mathcal{N}}} \sum_s \int \sqrt{|k|} dk c_{sk\sigma} + (t_{d1}/t_c) d_{1\sigma} \quad (10)$$

as the field operator accounting for the quantum state of the graphene site placed right beneath the tip with hopping terms ( $t_{d1}$  and  $t_c$ ), cf. Fig. 1. Therefore, the conductance through the graphene system at zero temperature  $T = 0$  is [1]:

$$G \sim \frac{e^2}{h} \Gamma_{\text{tip}} \text{LDOS}, \quad (11)$$

with  $\Gamma_{\text{tip}} = \pi t_c^2 \rho_{\text{tip}}$ ,  $\rho_{\text{tip}}$  as the STM tip DOS,

$$\text{LDOS} = -\frac{1}{\pi} \sum_\sigma \text{Im}[\tilde{\mathcal{G}}_\sigma(\varepsilon^+)] = 2\mathcal{D}_0 + \sum_{\sigma jl} \Delta \text{LDOS}_{jl\sigma} \quad (12)$$

stands for the total LDOS, where  $\tilde{\mathcal{G}}_\sigma(\varepsilon^+)$  is the time Fourier transform of  $\mathcal{G}_\sigma$ ,  $\mathcal{D}_0 = \frac{|\varepsilon|}{D^2}$  is the graphene DOS and the induced LDOS by the adatoms reads:

$$\Delta \text{LDOS}_{jl\sigma} = -(\pi v_0^2 \mathcal{D}_0^2) \text{Im}[(\mathcal{A}_l - i\mathcal{B}_l) \tilde{\mathcal{G}}_{d_{l\sigma} d_{j\sigma}} (\mathcal{A}_j - i\mathcal{B}_j)], \quad (13)$$

with  $\mathcal{A}_j = \frac{1}{\pi v_0^2 \mathcal{D}_0} \text{Re}\Sigma + \delta_{j1} (\pi^2 v_0^2 \mathcal{D}_0^2)^{-1/2} (t_{d1}/t_c)$  and  $\mathcal{B}_j = -\frac{1}{\pi v_0^2 \mathcal{D}_0} \text{Im}\Sigma$ .

**Results and Discussion.**— In the simulations we adopt the set of parameters:  $T = 0$ ,  $\varepsilon_{jd} = \varepsilon_d = -0.07D$ ,  $\mathcal{U} = v_0 = -2\varepsilon_d$ . Additionally, to avoid that BICs decay into the continuum, we use  $t_{d1}/t_c = 0$  [1].

In Fig. 2 we illustrate Eq. (3) for the single adatom version of the setup depicted in Fig. 1, which can be obtained by considering  $(\tilde{\Sigma}_{j\bar{j}}^{\bar{\sigma}} - \Sigma) \equiv 0$  in  $\mathcal{G}_{d_{1\sigma} d_{1\sigma}}$ . Panel (a) shows the local coupling regime  $q_0 = 0$  where  $v_F \sim c/300$ , which is in agreement with numerical renormalization group (NRG) results reported in Ref. [15] obeying the constraint  $2\varepsilon_d + \mathcal{U} = 0$  for the particle-hole symmetric case and  $T \rightarrow 0$ . It just exhibits the renormalized Hubbard bands in the vicinity of  $\bar{\varepsilon}_d$  and  $\bar{\varepsilon}_d + \mathcal{U} = -\bar{\varepsilon}_d$ . Consequently, this matching ensures that we can safely apply the Hubbard I method on graphene at  $T = 0$ . In the case of panel (b) we have  $q_0 = 1.2$  and  $v_F < c/300$  breaking

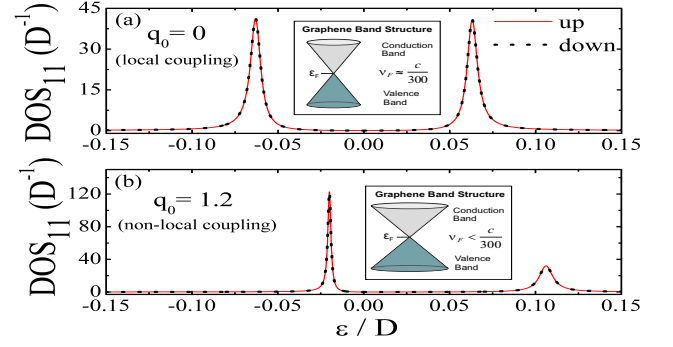


Figure 2: (Color online) DOS for the single adatom coupled to the graphene sheet. Two regimes are shown: (a)  $q_0 = 0$  corresponding to the local coupling and symmetric peaks at  $\bar{\varepsilon}_d$  and  $\bar{\varepsilon}_d + \mathcal{U} = -\bar{\varepsilon}_d$ . (b)  $q_0 \neq 0$  corresponding to non-local coupling and breaking of particle-hole symmetry.

the particle-hole symmetry of panel (a). The Fano factor  $q_0$  is increased by decreasing the slope of the Dirac cones when the Fermi velocity  $v_F$  is reduced as illustrated in the insets of both panels.

In Fig. 3(a) three distinct regions in the occupation numbers of Eq. (8) for  $j = 1, 2$  appear identified by their corresponding pseudogaps  $\Delta$  [Eq. (6)]: the non-magnetic regions corresponding to small or big Fano factors appear to be divided by a magnetic central domain delimited by the critical values  $q_{c1}$  and  $q_{c2}$ . At critical values, abrupt jumps in the occupation numbers point out the existence of a quantum phase transition connected with the spin degree of freedom. Panel (b) of the same figure presents the DOS corresponding to the regime  $q_0 = 0.8 < q_{c1}$  where one can clearly see resolved and spin-degenerate peaks in Eq. (3) for  $\text{DOS}_{jj}^\sigma$ . In Fig. 3(c) spin-polarized peaks emerge when the Fano factor is placed within the boundaries  $q_{c1} < q_0 = 1.2 < q_{c2}$ , while in panel (d) the case of  $q_0 = 2.0$  corresponds to the limit of the phantom atom considered in detail in Ref. [1] for which spin degeneracy is recovered.

To demonstrate that the system possesses BICs, we compare the density of states  $\text{DOS}_{jj}^\sigma$  for adatoms shown at Fig. 3 with the host local density of states  $\Delta \text{LDOS}_{jj\sigma}$  depicted at Fig. 4. As one can see, both quantities reveal pronounced peaks (resonant states) placed at the same positions. Particularly in panels (a) and (b) of Fig. 4, we observe as aftermath of Eq. (13), degenerate spin-up and down components for the Fano dips of  $\Delta \text{LDOS}_{jl\sigma}$  ( $l \neq j$ ) interfering destructively with the peaks found in  $\Delta \text{LDOS}_{jj\sigma}$ . As this interference is completely perfect, BICs emerge at the positions marked by vertical lines crossing panels (a), (b) and (c) of this figure. In panel (c), the total LDOS of Eq. (12) reveals absence of peaks at those places in which such a destructive interference occurs within panels (a) and (b). The aforementioned positions without peaks in Fig. 4(c) thereby give rise to

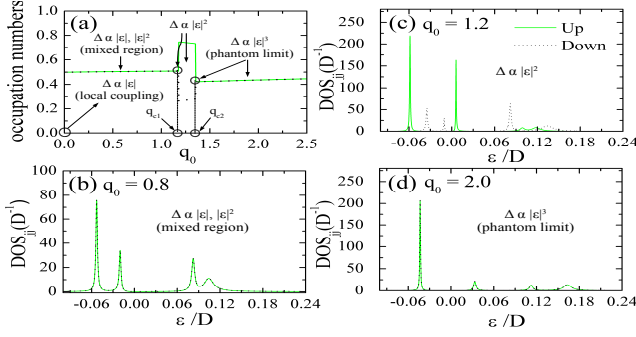


Figure 3: (Color online) Characteristic quantities of the graphene sheet with two adatoms (Fig.1): (a) occupation numbers given by Eq.(8) for spin-up and spin-down states of the adatoms as a function of  $q_0$ . The region corresponding to the magnetic BICs is characterized by abrupt jumps in the occupations. (b) DOS for the case  $q_0 < q_{c1}$ . Well resolved spin degenerate peaks are clearly visible. (c) DOS for the case  $q_{c1} < q_0 < q_{c2}$ . The peaks corresponding to the two spin components are distinct, which correspond to the lifting of spin degeneracy due to the onset of the effective exchange field between the adatoms. (d) DOS for the case  $q_0 > q_{c2}$  when spin degeneracy is recovered.

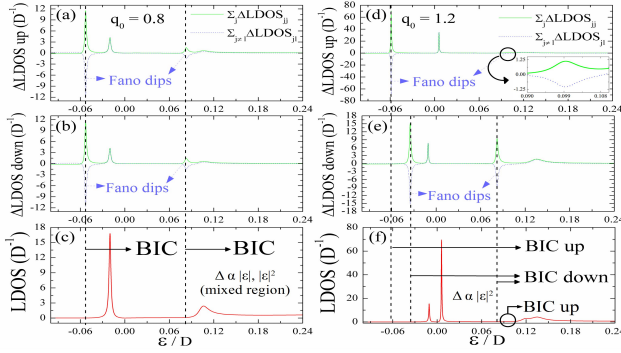


Figure 4: (Color online) Host local density of states corresponding to the cases of non-magnetic BICs (left panels (a), (b), and (c)) and magnetic BICs (right panels (d), (e) and (f)). BICs appear when a peak in  $\Sigma_j \Delta \text{LDOS}_{jj\sigma}$  is fully compensated by a Fano dip in  $\Sigma_{j \neq l} \Delta \text{LDOS}_{jl\sigma}$ . Positions of BICs are marked by vertical dashed lines. Panels (a), (b), (d) and (e) correspond to spin resolved  $\Delta$ LDOS. Lower panels (c) and (f) correspond to total LDOS defining the conductance.

BICs: the total LDOS that determines the conductance does not catch the same peaks found in Fig.3(b) for the adatoms. Thus the aforementioned invisibility of such resonant states points out that electrons with opposite spins stay equally trapped within these adatoms when  $q_0 < q_{c1}$  and the pseudogap scales as  $\Delta \propto |\epsilon|, |\epsilon|^2$ . Panels (d), (e) and (f) of Fig.4 correspond to the case  $q_{c1} < q_0 = 1.2 < q_{c2}$  where magnetic solutions become possible, since the pseudogap is ruled by  $\Delta \propto |\epsilon|^2$ . The position of magnetic BICs is denoted by vertical dashed lines.

Let us now present the physical arguments that elu-

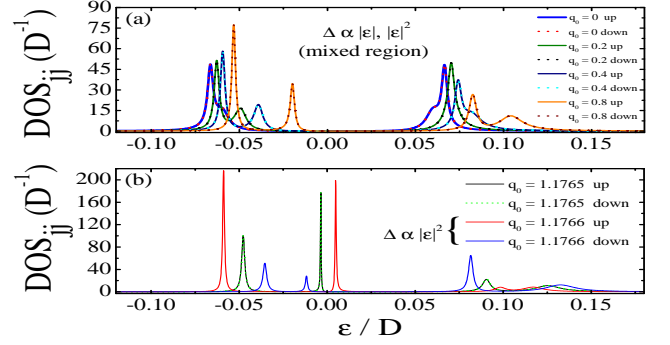


Figure 5: (Color online) (a) Spin-degenerate crossover from merged peaks of Eq.(3) for the adatoms DOS towards resolved peaks. (b) Quantum phase transition due to an abrupt spin-splitting of the peaks.

cidate the emergence of the reported magnetic BICs, which is indeed triggered by a quantum phase transition. Similar quantum phase transition appearing due to the quadratic scaling of the pseudogap  $\Delta \propto |\epsilon|^2$  and related breaking of the spin-degeneracy was discussed in Ref.[8], where a double dot system was explored. Fig. 5 illustrates how spin resolved DOS of the adatoms depend on the Fano parameter. The variation of  $q_0$  in the wide range below the critical value  $q_{c1} \approx 1.1766$  shifts the position of the peaks corresponding to opposite spin components equally, as it is shown in the upper panel of the figure. However, above the critical value the spin splitting abruptly appears as it is shown at the lower panel of the figure, which clearly indicates that the system undergoes a quantum phase transition. The abrupt appearance of the spin splitting is intimately connected with the step-like behavior observed in the occupation numbers shown in Fig.3(a). Note that the increase of the Fano factor above the second critical value  $q_{c2}$  leads to the recovering of the spin-degeneracy as the regime of the phantom atom with cubic scaling of the pseudogap  $\Delta \propto |\epsilon|^3$  is achieved.

Within the critical boundaries  $q_{c1} < q_0 < q_{c2}$ , the quantity  $\text{Re}(\tilde{\Sigma}_{jj}^{\sigma} - \Sigma) \equiv \mathcal{J}^{\text{exch}}$  from Eq.(9) plays the role of a Zeeman-like splitting of the levels  $\epsilon_d$  in the adatoms. This splitting arises from an intrinsic exchange field  $\mathcal{J}^{\text{exch}}$  between the adatoms intermediated by the graphene monolayer. Its value is ruled by the system natural order parameter, namely the Fano factor  $q_0$ , which drives the graphene system towards a quantum phase transition. As the upper and lower adatoms magnetize equally, cf. Fig.3(a), the coupling between them is revealed as ferromagnetic. Note that the dependence of the effective field on the Fano parameter is non-monotonous: it drops abruptly when  $q_0 = q_{c2}$ . We have verified that the values for the critical points  $q_{c1}$  and  $q_{c2}$  depend on the model parameters  $\epsilon_d, \mathcal{U}$  and  $v_0$ .

*Conclusions.*- In summary, we have proposed a setup

based on graphene-atom system in which magnetic BICs are triggered by a quantum phase transition in the region of the quadratic scaling of the pseudogap with energy,  $\Delta \propto |\varepsilon|^2$ . In this regime an effective ferromagnetic exchange field  $\mathcal{J}^{\text{exch}}$  between the adatoms mediated by graphene monolayer appears. The parameter which drives this transition is a Fano factor of interference tunable by changing the slope of the Dirac cones in graphene band-structure.

*Acknowledgments.*— This work was supported by CNPq, CAPES, 2014/14143-0 São Paulo Research Foundation (FAPESP), FP7 IRSES project QOCaN and Ranis project “Bose and Fermi systems for spintronics”. A. C. S. thanks the NTU at Singapore for hospitality. A. C. S. and M. d. S thank the Brazilian National Council for Scientific and Technological Development (CNPq).

- [1] L.H. Guessi *et al.*, Phys. Rev. B **92**, 045409 (2015).
- [2] W.-J. Gong *et al.*, Nanoscale Res. Lett. **8**, 330 (2013).
- [3] J. von Neumann and E. Wigner, Phys. Z. **30**, 465 (1929).
- [4] F.H. Stillinger and D.R. Herrick, Phys. Rev. A **11**, 446 (1975).
- [5] Y. Boretz *et al.*, Phys. Rev. A **90**, 023853 (2014).
- [6] A. Crespi *et al.*, Phys. Rev. Lett. **114**, 090201 (2015).
- [7] U. Fano, Phys. Rev. **124**, 1866 (1961).
- [8] L.G.G. V. Dias da Silva *et al.*, Phys. Rev. Lett. **97**, 096603 (2006).
- [9] P.W. Anderson, Phys. Rev. **124**, 41 (1961).
- [10] Z.-G. Zhu, K.-H. Ding, and J. Berakdar, Europhys. Lett. **90**, 67001 (2010).
- [11] A.C. Seridonio, M. Yoshida, and L.N. Oliveira, Europhys. Lett. **86**, 67006 (2009).
- [12] A.H. Castro Neto *et al.*, Rev. Mod. Phys. **81**, 109 (2009).
- [13] C. Hwang *et al.*, Sci. Rep. **2**, 590 (2012).
- [14] J. Hubbard, Proc. R. Soc. Lond. A, **281**, 401 (1964).
- [15] P.S. Cornaglia, G. Usaj, and C.A. Balseiro, Phys. Rev. Lett. **102**, 046801 (2009).

---

\* Current address: Institute of Semiconductor and Solid State Physics, Johannes Kepler University Linz, Austria.